Synchrotron Radiation Imaging Revealing the Sub-micron Structure of the Auditory Ossicles

Lukas Anschuetz[1], MD; Marco Dematté[1,2], MD; Alessia Pica[3], MD; Wilhelm Wimmer[4], PhD; Marco Caversaccio[1], MD; Anne Bonnin[5], PhD

[1] Department of Otorhinolaryngology, Head & Neck Surgery, Inselspital, Bern University Hospital, University of Bern, 3010 Bern, Switzerland

[2] Department of Otorhinolaryngology, Head & Neck Surgery, Head and Neck and Sensory Organs Department, Sant'Orsola-Malpighi Hospital, University of Bologna, Bologna, Italy

[3] Center for Proton Therapy, Paul Scherrer Institute, ETH Domain, Villigen, Switzerland

[4] Hearing Research Laboratory, ARTORG Center for Biomedical Engineering, University of Bern, Switzerland

[5] Swiss Light Source, Paul Scherrer Institut, Villigen, Switzerland

Funding Disclosure

No funding.

Conflict of Interest

The authors declare no conflict of interest.

Corresponding Author

Lukas Anschuetz, MD

Department of Otorhinolaryngology, Head & Neck Surgery, Inselspital, University Hospital and University of Bern, Freiburgstrasse, CH-3010 Bern, Switzerland

Email: anschuetz.lukas@gmail.com, Tel: +41 31 632 2654; Fax: +41 31 632 4872

Abstract

Purpose: Synchrotron-based X-ray Phase Contrast Imaging (SR X-PCI) allows, thanks to a highly coherent and powerful X-ray beam, the imaging of surface and cross-sectional tissue properties with high absorption-contrast. The objective of this study is to investigate the sub-micron structure of the ossicular chain. The understanding of its morphological properties at sub-micron scale will help to refine the understanding of its structural properties. The investigation of intact, non-decalcified and unstained ossicular bones allows to study the spatial relationship between surface properties, internal structure and tomographical slides.

Main results: The tomography datasets with a pixel size of 0.65 μm were reconstructed and 3D volume rendering models of all specimens were analyzed. Based on surface models, the surfaces of the articulations, the insertion of the tensor tympani and stapedial muscle tendons and the nutritional foramina, where the vessels penetrate the ossicles, were visualized. Moreover, a branched network of inner channels could be represented and its connection to the nutritional foramen was demonstrated.

Looking at the tomographic structure of the three ossicles a mineralization pattern for every auditory bone was described, indicating a considerable variation throughout the bones.

Conclusions: This study investigates the submicron-structure of the auditory ossicles at a pixel size of 0.65 μm, which is to the best of our knowledge the highest resolution reported in the investigation of the human auditory system so far. The provided data helps in the further understanding of the anatomical conformation of the ossicular chain.

Key words

Auditory ossicles; ossicular chain; synchrotron radiation; phase contrast imaging; vascular supply

Abbreviations

3D: three-dimensional

FE: finite element

CT: computed tomography

μCT: micro-computed tomography

SR X-PCI: synchrotron-based X-ray phase contrast imaging

Introduction

The middle ear has a highly complex anatomical structure and biomechanical function in amplifying and transmitting sound from the environment to the inner ear. Due to the small size of the auditory ossicles, the histopathological analysis has been the gold standard to describe the anatomy of its micro-structure as well as the related vascular supply (Nager and Nager, 1953; Hamberger, et al. 1963; Anson and Winch, 1974, Gulya and Schuknecht, 1995). Although highly accurate, this technique requires sectioning of decalcified tissue, which leads to sample destruction bearing the risk of structural deformation. Moreover, this process as well as three-dimensional (3D) reconstructions are highly time-consuming. The technique was used as a basis for finite element (FE) modelling of the middle ear structures (Gan, et al., 2002).

Developments in imaging technologies have made it possible to examine and reconstruct the ossicular chain in 3D, providing virtual information without the destruction of the sample. Clinically applicable computed tomography (CT) was used for modeling the middle ear and its biomechanics using FE analysis (Lee, et al., 2006). However, clinical CT images generally show a low spatial and contrast resolution. For higher spatial resolution, micro-computed tomography (μCT) was applied to the human ossicular chain, revealing its bony ossicular micro-structure. The reported pixel size is generally around 20 μm, varying between 10 and 80 μm (Decraemer, et al., 2003, De Greef, et al., 2015; Kaftan, et al., 2015). However, prior staining of the specimen, which is highly time consuming, may lead to tissue shrinkage (Buytaert, et al., 2014). A recent study compared a histo-anatomical micro-grinding method to unstained μCT-analysis and concluded that only histopathology is able to differentiate the anatomical structures such as the blood vessels, cartilaginous areas and collagen fiber direction inside the ossicles (Bradel, et al., 2017).

An imaging method allowing an even higher resolution is Synchrotron-based X-ray Phase Contrast Imaging (SR X-PCI). Thanks to the highly coherent and powerful X-ray beam

provided by the synchrotron, the X-ray images obtained contain information about the intensity attenuation and the phase shift of the X-ray beam when traversing the sample. The exploitation of those properties allows to increase the contrast on material that would appear uniform in conventional CT. The surface and cross-sectional tissue properties can be visualized, which permits the examination of the human middle ear with high absorption-contrast (Vogel and Schmitt, 1998; Vogel, 2000; Neudert, et al., 2010; Kanzaki, et al., 2011). The first investigation of middle ear structures of unstained, non-decalcified human temporal bones using SR X-PCI was published by Elfarnawany et al. (2017), reporting good visualization of bone and soft tissues with a voxel size around 9μm.

The objective of this study is to investigate the morphology of the ossicular chain using SR X-PCI. In this paper we present the first sub-micron resolution 3D volume obtained of the three bones of the human ossicular chain. The understanding of its morphological properties at a sub-micron scale will help to refine the understanding of its structural properties. As recently shown by Enghag et al. (2019) imaging at this accuracy paired with 3D-reconstructions is essential for further improving the understanding of middle ear sound transmission, pathophysiological mechanisms and surgical treatment by means of autologous or prosthetic ossicular replacements.

Materials and Methods

Ethical issues

The study protocol was approved by the local ethical committee (Kantonale Ethikkommission Bern, KEK-BE 2016-00887) and the local ethical committee for the Paul Scherrer Institute (Ethikkommission Nordwest- und Zentralschweiz, 2017-00805).

Sample preparation

The auditory ossicles (malleus, incus and stapes) were extracted from three Thiel-fixed (Thiel, 1992) human temporal bones taken from anonymous body donors using a predefined endoscopic approach to the middle ear (Anschuetz, et al., 2018). The samples were lesion free and without pathologies. After elevation of a tympano-meatal flap, the tympanic membrane was removed from the malleus separating the periosteum from the bone. Consecutively, the incudo-stapedial joint was sectioned and the incus removed and placed in a sterile container. Afterwards, the stapedial tendon was sectioned using a micro-scissor and the stapes was consecutively removed from the oval window using a 0.3mm micro-hook. Finally, the anterior malleolar ligament and the tendon of the tensor tympani muscle were cut and the hammer was taken from the middle ear. All ossicles were humified with physiological saline solution and stored in a fridge. The extracted ossicles underwent no further treatment before being scanned during the following week. The samples were fixed on the sample holder by using beeswax, a conventional method used for SR X-PCI.

Image acquisition

We have carried out synchrotron-based X-ray Phase Contrast Imaging tomography at the TOMCAT beamline (X02DA) of the Swiss Light Source (Paul Scherrer Institute, Switzerland). Due to the size of the samples, we performed a multiscale investigation, using two different X-ray propagation-based phase contrast imaging microscopes.

First, a “low” resolution (LR) setup was used to acquire an overview scan of the auditory ossicle. This setup consisted of a PCO 4.2 Edge camera combined with a 1:1 microscope. A YAG(Ce) (Yttrium Aluminum Garnet doped with Cerium) 250 μm thick scintillator was used to convert X-ray to visible light. With a 5.8 μm effective pixel size, the field of view (FoV) was 11.83 x 3.29 mm^2 and about 3 m propagation distance between the sample and the detector was used. Since the bones were larger than the FoV, vertical stitching scans with a 100

pixels overlap were performed to fully cover the samples. For each scan, 2501 projections were collected over 180°, on top of 20 darks and 2 series of 50 flats images (one before and one after the rotation). The exposure time was set to 50 ms, leading to about 5 min per scan. In a second step, high-resolution (HR) scans of the ossicles were performed. Because the FoV is too small to image each ossicle in one HR scan, each ossicle was imaged using multiple sub-scans. The region of interest (ROI) of each HR sub-scan was selected based on the reconstructed 3D LR dataset (Dejea, et al., 2019). The HR setup consisted of a PCO 5.5 Edge camera combined with a x10 microscope. A GGG:Eu ($Gd_3Ga_5O_{12}$ doped with Europium) 18 μm thick scintillator was used to convert X-ray to visible light. The exposure time was set to 100ms. For each sub-scan, 2501 projections were collected over 180°, on top of 20 darks and 2 series of 50 flats images (one before and one after the rotation) for a total acquisition time of 7min per scan. With a 0.65 μm pixel size, the FoV was 1.64 x 1.38 mm^2. In both cases, a 21 keV monochromatic X-ray beam was used. To reduce the X-ray dose on the bones, the sample alignment procedure was done using optical cameras and the acquisitions were performed by filtering the beam with a 5 mm Glassy Carbon (Sigradur) filter.

Reconstruction methodology

To correct for the inhomogeneities from the X-ray beam and dark current of the camera, the images were first flat-field corrected. Then, to remove the edge enhancement usually appearing in propagation-based phase contrast images, the Paganin's single-distance phase retrieval method was applied on the X-ray images (Paganin, et al., 2002). Phase retrieval methods allow to obtain the complex refractive index n of the sample, which can be written as $n = 1 - \delta + i\beta$, where δ represent the phase shift and β the absorption properties of the sample. Paganin, et al. (2002) developed a low pass filter where the delta/beta ratio is fine tuned to optimize the contrast in the images. The parameters used for the HR

acquisitions were δ=3.7e-8, β=1.7e-10 for a distance of 200mm. As this filter slightly deteriorates spatial resolution, we added a deconvolution step to restore it partially (Weitkamp, et al. 2013). A Gaussian deconvolution filter was employed, using a Gaussian width of 1 and a stabilizer of 0.3. The stabilizer is an additive offset in the filter and determines the trade-off between reduction of blurring and prevention of artefacts (Weitkamp, et al., 2013). Finally, the sinograms for each volume were computed and the reconstruction of the tomographic dataset was achieved using the Gridrec algorithm (Marone and Stampanoni, 2012), which is a modified faster version of the typical filtered back projection algorithm thanks to a regridding process to resample the Fourier space from polar to Cartesian coordinates. Reconstruction times were approximately 6.5 minutes with Paganin's method.

Stitching methodology

The reconstructed LR scans were stitched vertically using Matlab to obtain full 3D datasets of the entire bones. For the malleus, a total of four vertical scans were required, while for the incus three scans were done, and only two for the stapes. The reconstructed HR scans were stitched using NRStitcher, a Python stitching script internally developed at TOMCAT (Miettinen et al., 2019).

During the HR tomographic acquisition, motor movements are not exactly reproducible, and the sample can also slightly deform due to the long imaging times, leading to artefacts if using a rigid stitching procedure. NRStitcher is based on local phase correlation (i.e. elastic registration) and allows to detect the deformation and correct for it, leading to an artefact-free stitching 3D volume. To image the entire malleus, scans were made at seven heights along (say) the Y direction, and multiple scans were made at each height. The number of required scans in the X-Z plane at a certain height ranged from 1x1 to 3x3, where the two numbers indicate the amount of scans in the X and Z direction, respectively. For the stapes,

scans were made at three heights and the number of scans per height was 2x1, 2x1 and 3x2, respectively. For the incus, scans were made at five heights and the number of scans per height ranged from 1x1 to 3x5. As the full HR 3D volume was too heavy to handle efficiently (Malleus = 271 GB, Stapes = 101 GB, Incus =370 GB), we decided to work on height by height stitched volumes. Even with our Hewlett-Packard Z840 workstation customized with 512 GB RAM and two SSD drives of 500 GB, the computer was reaching is memory limit and Avizo, the software used for 3D rendering, was giving poor performance.

Results

A total of four auditory ossicles (one complete series of malleus, incus and stapes and an additional incus) were extracted and scanned.

Three-dimensional surface and internal structure

The tomography datasets were reconstructed and 3D volume rendering models of all specimens were analyzed (Figure 1). Based on these surface models, the anatomical structure and smallest details of every ossicle could be studied. Of particular interest were the surfaces of the articulations (incudo-malleolar and incudo-stapedial), the insertion of the tensor tympani and stapedial muscle tendons and the nutritional foramina, where the vessels penetrate the ossicles. However, strictly speaking this functional property of the observed branched network cannot be deducted from the present investigation. The diameters of the foramina indicated in Figure 1 were measured and revealed a mean diameter of 182 μm ranging from 69 to 388 μm. From the surface properties, zones of porous surface structure were observed especially on the medial side of the malleus, on the medial side of the long process of the incus and on the posterior and inferior part of the neck of the stapes.

Several nutritional foramina were identified: the anterior surface of the malleus head (posterior tympanic artery), malleus neck (malleolar branch of the anterior tympanic artery), lateral side of the incus body, near the base of the long crus and close to the articulation area with the malleus (incudal branch of the anterior tympanic artery), base of the long crus (posterior tympanic artery) and medial side at the base of the short crus (superior main branch of the anterior tympanic artery). In Figure 2, the internal structure of the ossicles is highlighted with isosurface rendering, and the outer surface of the ossicles is added in semi-transparent color. A branched network of inner channels could be identified. The head of the malleus and the body of the incus contain the largest channels. Branches of intermediate size were found in the short and long process of the incus, as well as in the handle of the malleus. On the stapes a small lacune was identified on the anterior side of the capitulum traversing the neck and giving a branch to the posterior crus, which gives a branch to the footplate. Further analysis revealed a connection of the nutritional foramen on the incus to this internal structure indicating the function of blood supply to the bone of this branched network inside the ossicles (Figure 3).

Tomographic structure

On the HR tomographic images with a pixel size of 0.65 μm the nano-structure of the bones and soft-tissue components inside the ossicles can be studied. The difference of contrast provides information regarding the bone density and mineralization level. Darker areas correspond to a low absorbing part (black corresponds to air) while whiter areas correspond to a denser part, such as bone. In Figure 4, the left image corresponds to the LR 3D volume rendering with internal isosurface of the malleus. The four images on the right correspond to HR selected slices of the full HR volume, taken at four different heights as represented by colors. The darker areas, i.e. porosities, seen inside the bones on the HR slices correspond to the areas highlighted with the isosurface rendering on the LR 3D rendering.

Those black parts represent the above-mentioned cavities inside the bones and contain the nutritional blood vessels. Looking at the tomographic structure of the malleus we observe a higher mineralization level in the handle as compared to the body, which contains more nutritional cavities. Moreover, an irregular but consistently higher mineralization level at the periphery of the bone is observed. The thickness of these higher density zones varies considerably but appears to be most consistent on the superior and inferior parts of the bone. For the incus a similar picture is observable. On Figure 5, the left side represents the 3D rendering of the incus with the internal structure highlighted. On the right, Figure 5b-c are HR images obtained for the cross section on the lenticular process of the incus (i.e. vertical virtual cut) and 2 cross sections taken at two different heights represented on Figure 5a. We found zones of lower mineralization especially around the lacunes in the periphery of the incudal body. Moreover, the long process and especially the transition zone to the lenticular process shows lower bone densities. Figure 6a shows a 3D volume rendering of the stapes. Figure 6b and 6c are HR slices. Figure 6b is a vertical virtual cut parallel to the area represented with the white square in Figure 6a, while Figure 6b is a slice taken in the footplate of the stapes (blue dotted line in Figure 6a). As shown in Figure 6, the tomographical images of the stapes show a rather homogeneous picture of low-density bone.

Discussion

This study investigated the sub-micron structure of the auditory ossicles using SR X-PCI. Those high-resolution images scanned at a pixel size of 0.65 μm are to the best of our knowledge the highest resolution reported in the investigation of the human auditory system so far. Kanzaki et al. (2011) reported an effective voxel size of 0.22 μm in the investigation of the auditory ossicels of osteopetrotic mice. The investigation of intact, non-decalcified and unstained ossicular bones allows to study the spatial relationship between surface

properties, internal structure and tomographical slides. However, the findings are based on a small sample size and should be interpreted in this regard.

Ossicular chain blood supply

The description of the main blood supply of the ossicular chain is historically based on histological section techniques described by several authors (Nager and Nager, 1953; Hamberger, et al., 1963; Lindeman 1964; Anson and Winch, 1974; Lanniga, et al., 1993). The anterior tympanic artery divides into two main nutrient branches: one branch runs inside the anterior malleolar plication and divides into two vessels: one for the malleus penetrating the bone through two nutrient foramina at the lateral part of the malleus' neck and the other for the blood supply of the incus (see below). The other branch of the anterior tympanic artery runs to the superior malleolar ligament and reaches the malleus through the plication of this ligament at the head of the malleus. The posterior tympanic artery also branches to the malleus, near the medial part of the malleus' neck. It runs only shortly along the bone surface and then penetrates it through a nutrition foramen on the medial side of the malleus. Three blood vessels penetrate the incus through nutrition foramina. The main blood vessel derives from the incudal branch of the anterior tympanic artery. This blood vessel reaches the incus on the lateral side of the body, near the base of the long crus and close to the articulation area with the malleus. From the posterior tympanic artery, a branch with large diameter leaves the blood vessel near the incudo-stapedial joint and runs on the medial side of the incus' mucosa to the base of the long crus where it enters the bone. The third main blood vessel reaches the incus on the medial side at the base of the short crus and penetrates the bone through another nutrition foramen. This blood vessel is a branch of the superior main branch of the anterior tympanic artery and runs through the plication of the superior incudal ligament.

Our findings regarding nutritional foramina concur with the above-mentioned historical literature and also with recently described microgrinding techniques (Bradel, et al., 2017). Strictly speaking, from our results the definitive function of these openings may not be claimed. However, this interpretation of our data appears to agree with the existing literature and especially histological investigations. Moreover, from the isosurface renderings a more branched penetration may be expected due to a higher number of observed nutritional foramina. With a mean diameter of 182 μm these openings are similar in size to those observed in the mastoid air cell system (mean 158 μm) as described by Cros, et al. 2013. This finding emphasizes the importance of the extensive network of mucosal nutrient vessels on the surface of the auditory ossicles (Hamberger, et al., 1963), which is deemed particularly important for the vascularization of the processes of the incus and malleus. A recent in-vivo study examined the direction of blood flow in these mucosal vessels by direct intraoperative endoscopic observation in patients and found a multidirectional pattern of blood flow. For instance, the blood flow direction of the incudo-stapedial artery is described in 80% of individuals from the incus to the stapes, but in 20% of individuals the blood flows from the stapes to the incus (Alicandri-Ciufelli, et al., 2018).

The blood supply of the stapes varies from the other two ossicles (Nager and Nager, 1953; Alberti, 1963). The posterior tympanic artery runs over the incudostapedial joint and gives a rich blood vessel supply to the mucosa of the capitulum, which form branches running along the inner surface of the u-shaped anterior and posterior crus in the direction of the footplate. The branch leading to the head of the stapes penetrates the bone through a nutrition foramen on the anterior side of the head and runs through the bone, leaving it to join the blood vessel on the inner surface of the crura. On the footplate of the stapes there are only a few fine blood vessels within the mucosal layer. Along the annular ligament of the stapes a vascular ring is located. It is supposed that, due to the small size of the crura, the nutrition takes place through diffusion. In lamellar bone the maximal diffusion distance is about 150

µm (Hamberger and Wersaell, 1964). In contrast, our results suggest the presence of a lacune in the stapes head, which is branched to the posterior crus until reaching the footplate. Whether this represents a nutritional vessel inside the posterior crus has to be further investigated.

Surface structure and isosurface renderings

The surface and collagen fiber arrangement of the auditory ossicles has been studied using electron microscopy by various authors (Hassmann and Chodynicki, 1978; Zenev, et al., 2006; Chen, et al., 2008). Chen et al. (2008) described bone resorption zones around the nutritional foramina, on the long process of the incus and on the neck of the stapes. These findings could be reproduced using SR X-PCI with additionally identified porous surfaces on the medial side of the malleus. Moreover, as observable on the HR tomography slides the bone density is decreased around the vascular inlets on the bone surface (see below). The etiology of these porous surfaces may be related to an increased bone turnover around the vascular openings possibly due to calcium exchange (Chen, et al, 2002). However, the ossicles and especially the long process of the incus are subject to changes in their bony structure with age, which may be maladaptive (Lannigan, et al., 1995). As the specimens derived in this investigation are from anonymous body donors, the assessment of age was not possible. It is however very probable that these ossicles were from older subjects. Yet, it would be very interesting to further investigate the difference of bone surface structures related to age.

Tomographic imaging

From the HR tomographical slides of all three ossicles, zones of various X-ray absorption and therefore mineral density were identified. Zones of smaller density were observed especially around the vascular structures like the nutritional foramina on the surface, as well

as around the internal vascular channels. This association may be best explained by ongoing bone turnover, which of course requires adequate blood supply (Chen, et al., 2002). Moreover, the observation of decreased bone density around the long process and especially the lenticular process of the incus is interesting as it correlates to the zones of porous surface structure. In fact, the long process of the incus is most often subject to pathological bone resorption leading to conductive hearing loss occurring in chronic otitis media (Albera, et al., 2015). This correlation of altered surface structure and decreased bone density could be explained by the bone resorption mechanisms around vascular structures (Chen, et al., 2002). However, the investigation of Morris et al. (2018) suggests decreased bone mineral density at sites of highest biomechanical stress, as no statistically significant variation in bone density related to age was observed. Similarly, the authors describe low mineralization at the attachment site of the stapedial tendon. Our results suggest a similar finding as a porous surface structure was observed at the stapedial tendon insertion.

Regarding mineralization of the auditory ossicles, the study by Kanzaki et al. (2011) investigated osteopetrotic mice with SR tomographic microscopy among other techniques. They observed a decreased volume of the tympanic cavity with concomitant enlarged auditory bones in osteopetrotic mice compared to healthy subjects. Therefore, bone resorption mechanisms are important to allow the ossicles inside the tympanic cavity to vibrate freely. This is particularly interesting as constant bone remodeling appears to be dependent on the vascular supply and therefore deserves in our opinion a more detailed scientific attention, especially in the context of surgical repair of ossicular chain discontinuity.

Conclusion

This study investigates the submicron-structure of the auditory ossicles at a pixel size of 0.65 um, which are to the best of our knowledge the highest resolution reported in the

investigation of the human auditory system so far. The provided data helps in the further understanding of anatomical conformation of the ossicular chain.

Acknowledgements

We acknowledge the Paul Scherrer Institut, Villigen, Switzerland for provision of synchrotron radiation beamtime at the TOMCAT beamline X02DA of the SLS.

References

1. Albera R, Dagna F, Filippini C, Albera A, Canale A., 2015. Ossicular Chain Lesions in Tympanic Perforations and Chronic Otitis Media without Cholesteatoma. J Int Adv Otol. Aug;11(2):143-6.
2. Alberti PW., 1963. The blood supply of the incudostapedial joint and the lenticular process. Laryngoscope. May;73:605-28.
3. Alicandri-Ciufelli M, Guarino P, Fabbri F, Cunsolo EM, Presutti L, Anschuetz L., 2018. Middle ear microvascularization: an "in vivo" endoscopic anatomical study. Eur Arch Otorhinolaryngol. Apr;275(4):889-894.
4. Anschuetz L, Presutti L, Marchioni D, Bonali M, Wimmer W, Villari D, Caversaccio M., 2018. Discovering Middle Ear Anatomy by Transcanal Endoscopic Ear Surgery: A Dissection Manual. J Vis Exp. Jan 11;(131). doi: 10.3791/56390.
5. Anson BJ, Winch TR., 1974. Vascular channels in the auditory ossicles in man. Ann Otol Rhinol Laryngol. Mar-Apr;83(2):142-58.
6. Bradel S, Doniga-Crivat L, Besdo S, Lexow F, Fehr M, Lenarz T, Prenzler N, Brandes G., 2017, Innovative 3D Model of the Human Middle Ear in High Resolution with a Histological Microgrinding Method: A Feasibility Study and Comparison with μCT. Int J Otolaryngol. 2017:6753604.
7. Buytaert, J., Goyens, J., De Greef, D., Aerts, P., Dirckx, J., 2014. Volume shrinkage of bone, brain and muscle tissue in sample preparation for micro-CT and light sheet fluorescence microscopy (LSFM). Microsc. Microanal. 20, 1208e1217.
8. Chen H, Hayakawa D, Emura S, Ozawa Y, Okumura T, Shoumura S., 2002. Effect of low or high dietary calcium on the morphology of the rat femur. Histol. Histopathol. 17:1129–1135.

9. Chen H, Okumura T, Emura S, Shoumura S., 2008. Scanning electron microscopic study of the human auditory ossicles. Annals of Anatomy 190(1): 53–58.

10. Cros O, Borga M, Pauwels E, Dirckx JJ, Gaihede M., 2013. Micro-channels in the mastoid anatomy. Indications of a separate blood supply of the air cell system mucosa by micro-CT scanning. Hear Res. Jul;301:60-5. doi: 10.1016/j.heares.2013.03.002. Epub 2013 Mar 19.

11. Decraemer WF, Dirckx JJ, Funnell WR., 2003. Three-dimensional modelling of the middle-ear ossicular chain using a commercial high-resolution X-ray CT scanner. J Assoc Res Otolaryngol. Jun;4(2):250-63.

12. De Greef D, Buytaert JA, Aerts JR, Van Hoorebeke L, Dierick M, Dirckx J., 2015. Details of human middle ear morphology based on micro-CT imaging of phosphotungstic acid stained samples. J Morphol. Sep;276(9):1025-46.

13. Dejea H, Garcia-Canadilla P, Cook AC, Guasch E, Zamora M, Crispi F, Stampanoni M, Bijnens B, Bonnin A., 2019. Comprehensive Analysis of Animal Models of Cardiovascular Disease using Multiscale X-Ray Phase Contrast Tomography. Sci Rep. May 6;9(1):6996.

14. Elfarnawany M, Rohani SA, Ghomashchi S, Allen DG, Zhu N, Agrawal SK, Ladak HM., 2017. Improved middle-ear soft-tissue visualization using synchrotron radiation phase-contrast imaging. Hear Res. Oct;354:1-8. doi:10.1016/j.heares.2017.08.001.

15. Enghag S, Strömbäck K, Li H, Rohani SA, Ladak HM, Rask-Andersen H, Agrawal S., 2019. Incus Necrosis and Blood Supply: A Micro-CT and Synchrotron Imaging Study. Otol Neurotol. May 6. doi: 10.1097/MAO.0000000000002292. [Epub ahead of print]

16. Gan RZ, Sun Q, Dyer RK Jr, Chang KH, Dormer KJ., 2002. Three-dimensional modeling of middle ear biomechanics and its applications. Otol Neurotol. May;23(3):271-80.

17. Gulya AJ, Schuknecht HF., 1995. Anatomy of the Temporal Bone with Surgical Implications. New York: Parthenon Pub. Group.

18. Hamberger CA, Marcuson G, Wersäll J., 1963. Blood vessels of the ossicular chain. Acta Otolaryngol Suppl. 183:6-70.

19. Hamberger CA, Wersaell J., 1964. Vascular supply of the tympanic membrane and the ossicular chain. Acta Otolaryngol Suppl. 188:SUPPL 188:308+

20. Hassmann E, Chodynicki S., 1978. Scanning electron microscopy of human ossicles. Archives of Oto-Rhino-Laryngology. 220(3): 175–185.

21. Kaftan H, Böhme A, Martin H., 2015. Geometric parameters of the ossicular chain as a function of its integrity: a micro-CT study in human temporal bones. Otol Neurotol. Jan;36(1):178-83.

22. Kanzaki, S., Takada, Y., Niida, S., Takeda, Y., Udagawa, N., Ogawa, K., Nango, N., Momose, A., Matsuo, K., 2011. Impaired vibration of auditory ossicles in osteopetrotic mice. Am. J. Pathol. 178, 1270e1278. http://dx.doi.org/10.1016/j.ajpath.2010.11.063.

23. Lannigan FJ, O'Higgins P, Oxnard CE, McPhie P., 1995. Age-related bone resorption in the normal incus: a case of maladaptive remodelling? J. Anat. 186, 651–655.

24. Lannigan FJ, O'Higgins P, McPhie P., 1993. The vascular supply of the lenticular and long processes of the incus. Clin Otolaryngol Allied Sci. Oct;18(5):387-9.

25. Lee CF, Chen PR, Lee WJ, Chen JH, Liu TC., 2006. Three-dimensional reconstruction and modeling of middle ear biomechanics by high-resolution

computed tomography and finite element analysis. Laryngoscope. May;116(5):711-6.

26. Lindeman H., 1964. Some histological examinations of the incus and stapes with especial regard to their vascularization. Acta Otolaryngol Suppl. 188:SUPPL 188:319+.

27. Marone F, Stampanoni M., 2012. Regridding reconstruction algorithm for real-time tomographic imaging. J. Synchrotron Rad. 19, 1029-1037

28. Miettinen A, Oikonomidis IV, Bonnin A, Stampanoni M., 2019. NRStitcher: Non-rigid stitching of terapixel-scale volumetric images. Bioinformatics. May 22. pii: btz423. doi: 10.1093/bioinformatics/btz423. [Epub ahead of print]

29. Morris C, Kramer B, Hutchinson EF., 2018. Bone mineral density of human ear ossicles: An assessment of structure in relation to function. Clin Anat. Nov;31(8):1158-1166. doi: 10.1002/ca.23231. Epub 2018 Sep 3. PubMed PMID: 30178530.

30. Nager GT, Nager M., 1953. The arteries of the human middle ear, with particular regard to the blood supply of the auditory ossicles. Ann Otol Rhinol Laryngol. Dec;62(4):923-49.

31. Neudert M, Beleites T, Ney M, Kluge A, Lasurashvili N, Bornitz M, Scharnweber D, Zahnert T., 2010. Osseointegration of titanium prostheses on the stapes footplate. J. Assoc. Res. Otolaryngol. 11, 161-171.

32. Paganin D, Mayo SC, Gureyev TE, Miller PR, Wilkins SW., 2002. Simultaneous phase and amplitude extraction from a single defocused image of a homogeneous object. J Microsc. Apr;206(Pt 1):33-40.

33. Thiel W., 1992. The preservation of the whole corpse with natural color (in German). Ann Anat. 174:185 – 95.

34. Vogel U, Schmitt T., 1998. 3D visualization of middle ear structures. In: Kim, Y., Mun, S.K. (Eds.). SPIE Med. Imaging. International Society for Optics and Photonics, pp. 141e151. http://dx.doi.org/10.1117/12.312487.

35. Vogel, U. 3D-imaging of internal temporal bone structures for geometric modelling of the human hearing organ., 2000. In: Wada, H., Takasaka, T., Ikeda, K., Ohyama, K., Koike, T. (Eds.), Recent Developments in Auditory Mechanics. World Scientific Publishing, River Edge, NJ, pp. 44-50.

36. Weitkamp T, Haas D, Rack A., 2013.ANKAphase user guide. http://rsbweb.nih.gov/ij/plugins/ankaphase/ankaphase-userguide.html—sec:restor

37. Zenev I, Zenev E, Sapundzhiev N, Milkov M, Marev D., 2006. Scanning electron microscopy of auditory ossicles. The Mediterranean Journal of Otology. 3: 112–116

Figure Legends

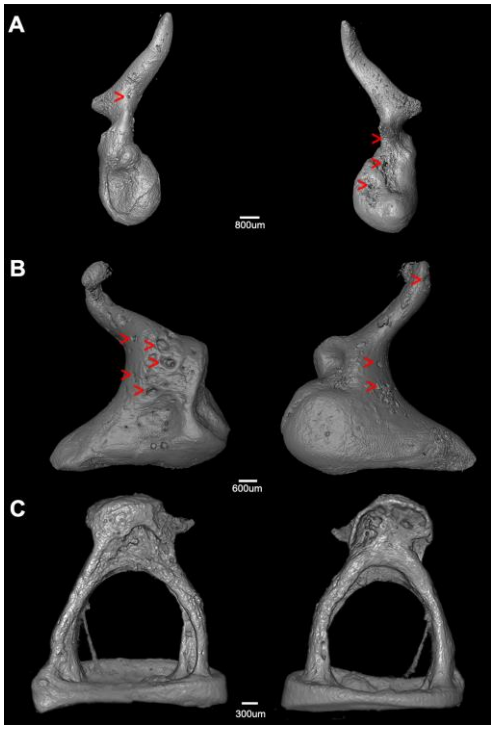

Figure 1: 3D volume rendering

3D reconstructions of a right ossicular chain in volume renderings. Panel A: malleus from lateral left and medial right; B: incus from inferior left and superior right and C: stapes view from superior left and inferior right. Arrowheads exemplarily indicate nutritional foramina.

Figure 2: 3D isosurface rendering

Illustration of branched internal network bearing nutritional vessels of a right ossicular chain. Panel A: malleus from lateral left and medial right; B: incus from inferior left and superior right and C: stapes view from superior left and inferior right. Arrowheads: small lacune on the anterior side of the capitulum traversing the neck and giving a branch to the posterior crus and to the footplate.

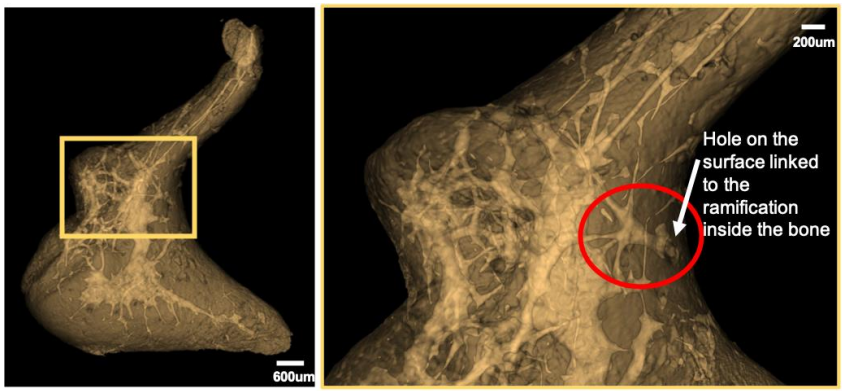

Figure 3: Association of nutritional foramen and internal network

Right incus with detailed view of superficial holes (nutritional foramina) linked to the internal network.

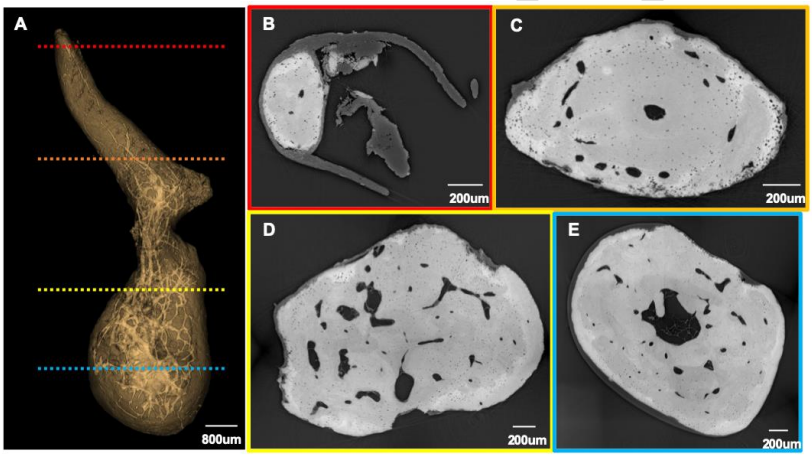

Figure 4: Tomographic images of a right malleus

3D reconstruction of a right malleus on the left side with high-resolution tomographic sections taken on different heights as indicated by colors.

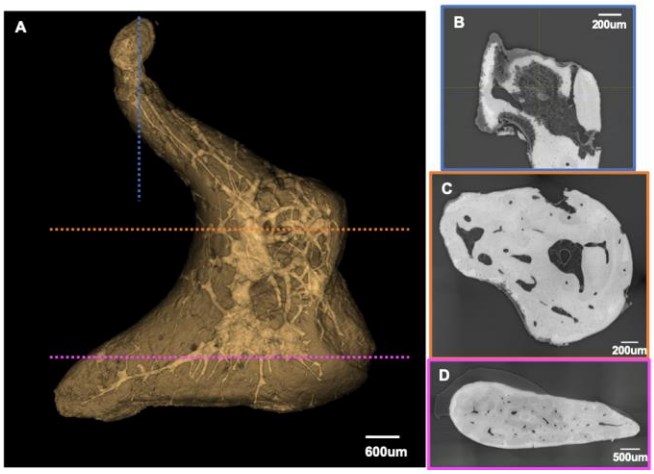

Figure 5: Tomographic images of a right incus

3D reconstruction of a right incus on the left side with high-resolution tomographic sections taken on different heights as indicated by colors. Section of the lenticular process in sagittal plane.

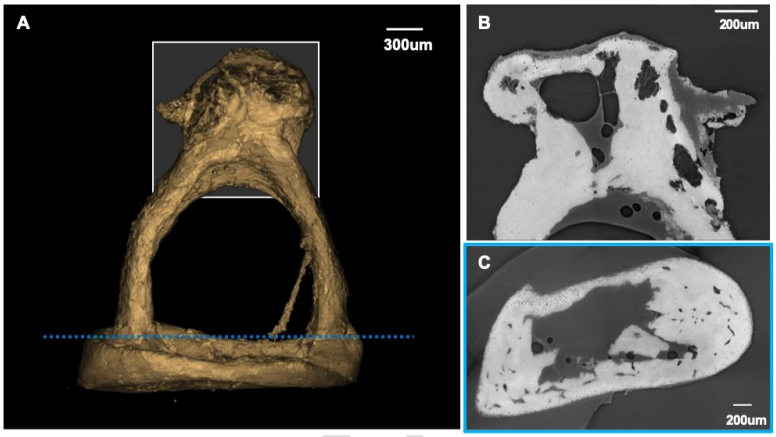

Figure 6: Tomographic images of a right stapes

3D reconstruction of a right stapes on the left side with high-resolution tomographic sections taken in frontal plane trough the capitulum and in horizontal plane trough the footplate.